Scientific Report

TRANSPARENT PROCESS

EMBO reports

Antagonistic functions of *LMNA* isoforms in energy expenditure and lifespan

Isabel C Lopez-Mejia[1,2,†], Marion de Toledo[1,†], Carine Chavey[1], Laure Lapasset[1], Patricia Cavelier[1], Celia Lopez-Herrera[1], Karim Chebli[1], Philippe Fort[3], Guillaume Beranger[4], Lluis Fajas[2], Ez Z Amri[4], François Casas[5] & Jamal Tazi[1,*]

Abstract

Alternative RNA processing of *LMNA* pre-mRNA produces three main protein isoforms, that is, lamin A, progerin, and lamin C. *De novo* mutations that favor the expression of progerin over lamin A lead to Hutchinson-Gilford progeria syndrome (HGPS), providing support for the involvement of *LMNA* processing in pathological aging. Lamin C expression is mutually exclusive with the splicing of lamin A and progerin isoforms and occurs by alternative polyadenylation. Here, we investigate the function of lamin C in aging and metabolism using mice that express only this isoform. Intriguingly, these mice live longer, have decreased energy metabolism, increased weight gain, and reduced respiration. In contrast, progerin-expressing mice show increased energy metabolism and are lipodystrophic. Increased mitochondrial biogenesis is found in adipose tissue from HGPS-like mice, whereas lamin C-only mice have fewer mitochondria. Consistently, transcriptome analyses of adipose tissues from HGPS and lamin C-only mice reveal inversely correlated expression of key regulators of energy expenditure, including Pgc1a and Sfrp5. Our results demonstrate that *LMNA* encodes functionally distinct isoforms that have opposing effects on energy metabolism and lifespan in mammals.

Keywords aging; energy expenditure; LMNA protein isoforms; mitochondria biogenesis; RNA processing

Subject Categories Metabolism; Physiology

DOI 10.1002/embr.201338126 | Received 18 October 2013 | Revised 7 February 2014 | Accepted 11 February 2014 | Published online 17 March 2014

EMBO Reports (2014) 15: 529–539

See also: **IA Chatzispyrou & RH Houtkooper** (May 2014)

Introduction

Multiple signaling pathways affect senescent decline and aging. Studies in simple model organisms have led to remarkable progress in understanding the molecular pathways that modulate aging and senescence [1–3]. However, the mechanisms mediating senescent decline and aging in mammals remain unclear. Thus, it is important to understand which cells or tissues coordinate the aging process at the level of the whole organism.

The Hutchinson-Gilford progeria syndrome (HGPS or progeria) is a rare syndrome that causes premature aging [4]. Progeria is typically due to a silent *de novo* mutation in exon 11 of the *LMNA* gene (1824C > T, G608G). This mutation increases the usage of a natural splice donor site in exon 11 of *LMNA* [5–7], leading to an in-frame deletion of 150 nucleotides, including the cleavage motif required for the last maturation step of lamin A by the ZMPSTE24 endoprotease [8]. Both *Zmpste24*-deficient mice ($Zmpste24^{-/-}$) and farnesylated progerin ($Lmna^{HG/+}$) knock-in mice present HGPS-like phenotypes [8,9], implying that defects in prelamin A processing rather than the loss of lamin A are responsible for premature aging. Interestingly, knock-in mouse models lacking either the lamin A (lamin C-only) or lamin C (lamin A-only) isoform do not exhibit disease phenotypes [9,10].

The RNA processing mechanisms leading to progerin and lamin C production are highly conserved in humans and mice [7,10,11]. Lamin C has not yet been identified outside of the mammalian lineage (Fig 1, [8,11]), and the polyadenylation site responsible for lamin C production is conserved between mammals. Since progerin expression is mutually exclusive with lamin C expression, we examined whether lamin C and progerin have opposite effects on lifespan. *Lmna* knock-in mice in which *Lmna* exons 11 and 12 are not transcribed and thus progerin-specific splicing cannot be performed were used in this study. Our results show that lamin C and progerin trigger antagonistic signals in adipose tissue that regulate mitochondrial biogenesis and energy expenditure. This study introduces a characterization of lamin C-only-expressing mouse model that exhibits obese phenotypes and increased lifespan.

1 Institut de Génétique Moléculaire de Montpellier, CNRS UMR 5535, Universities of Montpellier 1 and Montpellier 2, Montpellier, France
2 Département de Physiologie, Université de Lausanne, Lausanne, Switzerland
3 CNRS, Centre de Recherche de Biochimie Macromoléculaire de Montpellier, Montpellier, France
4 Faculté de Médecine, Inserm U844, Institut de Biologie de Valrose, UMR CNRS 7277 – UMR INSERM 1091, Universit de Nice Sophia Antipolis, Nice, France
5 UMR Dynamique Musculaire et Métabolisme, NRA - CAMPUS SUPAGRO 2 place Viala, Montpellier, France
*Corresponding author. Tel: +33 4 34 359685; Fax: +33 4 34 359634; E-mail: jamal.tazi@igmm.cnrs.fr
†These authors contributed equally to this work.

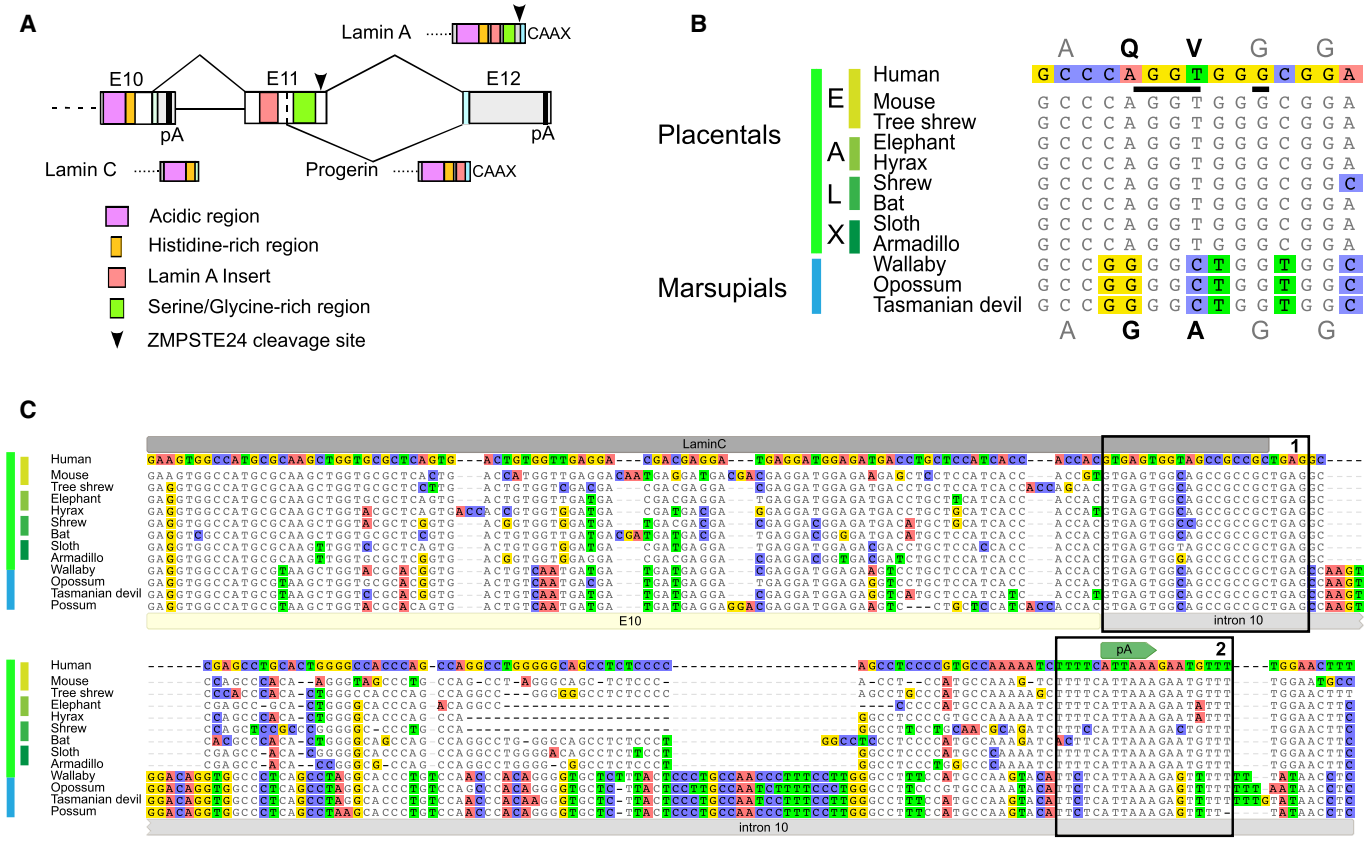

E Occurrence of LaminA and LaminC ESTs in databases

Species	LaminA+C[a]	Lamin A[b]	Lamin C[c]
Human	>1000	>500	>500
Rattus norvegicus	30	12	14
Bos taurus	71	17	42
Sus scrofa	79	9	45
Marsupials	5	2	1
Gallus gallus	3	3	0
Xenopus	13	13	0
Fish	12	12	0

[a] Number of laminA ESTs in databases
[b] ESTs containing E10 and/or E11 exons
[c] ESTs containg Exon10 and intron 10

Figure 1. *LMNA* RNA processing isoforms during evolution.

A Schematic view of the three variable C-termini produced by the *LMNA* locus. Only the region spanning over exon 10 (E10), intron 10, exon 11 (E11), intron 11, and exon 12 (E12) is presented. pA are the polyadenylation sites producing lamin C and lamin A.

B The alignment of progerin 5′ splice site shows that it is conserved in the four placental super-orders (E: Euarchontoglires; A: Afrotheria; L: Laurasiatheria; X: Xenarthra).

C Lamin C is conserved in Therians. Alignment of the genomic sequences spanning over exon 10 and the 5′ end of intron 10 (IVS 10). Boxes labeled 1 and 2 show the high levels of conservation of the exon/intron borders and polyadenylation signals, respectively.

D Alignment of the amino acids encoded by the genomic sequences (end of exon 10 and beginning of intron 10) shown in (C).

E Occurrence of lamin A and lamin C ESTs in databases.

Results and Discussion

Complexity of the C-terminus of lamin A during evolution

In order to infer functional relationship between *LMNA* isoforms, we first examined when production of progerin and lamin C isoforms was selected during evolution. We found that the splice site responsible for progerin production is included in a region highly conserved throughout the four placental super-orders but absent in the exon 11 sequences of marsupials from three distinct orders (Fig 1B). In contrast, lamin C transcripts and a conserved polyadenylation signal site in intron 10 were identified in all placentals and marsupials examined (Fig 1C–E). Furthermore, intron 10 nucleotide sequences proximal to the splice sites (Fig 1C) and the corresponding encoded peptides (Fig 1D) showed extreme conservation. This supports a scenario in which lamin C production was selected first in mammals, followed by progerin in placentals. Lamin C lacks the residues encoded by exons 11 and 12 of the *LMNA* gene; therefore, the complex maturation process involving proteolytic cleavage of the C-terminal part of prelamin A does not occur. Failure of prelamin A processing leads to the progeroid phenotype [8,12]; thus, the production of lamin C by alternative RNA processing may be an evolutionary adaptation to counteract the deleterious effects that result from inefficient prelamin A maturation. This also suggests that the production of *LMNA* isoforms may have physiological outcomes. This hypothesis was further tested here using mouse models.

Lifespan and growth of mice carrying different *Lmna* alleles

The first mouse model of progeria to recapitulate the premature aging phenotype and splicing alteration observed in HGPS was recently described [7,10]. The progeria allele ($Lmna^{G609G}$ allele) was created by a knock-in strategy involving another mutant allele that encodes lamin C alone ($Lmna^{LCS}$ allele). This allele carries a floxed neo cassette just downstream of the polyadenylation site of lamin C and the G609G mutation in exon 11 (Fig 2A). $Lmna^{G609G/+}$ and $Lmna^{LCS/+}$ mice were intercrossed to generate $Lmna^{G609G/G609G}$, $Lmna^{G609G/+}$, $Lmna^{LCS/+}$, and $Lmna^{LCS/LCS}$ mice used in this study. $Lmna^{+/+}$ obtained from both crosses were used as controls. Specific *Lmna* isoform expression was confirmed by Western blot (Fig 2A, and [7,10]).

As expected, mice homozygous for the G609G mutation lived < 6 months. In contrast, mice carrying only one G609G allele lived for 1 year on average. Most of the control mice died after 2 years, whereas approximately 60% of the $Lmna^{LCS/+}$ and $Lmna^{LCS/LCS}$ mice remained alive (Fig 2B). The median lifespan of $Lmna^{LCS/+}$ and $Lmna^{LCS/LCS}$ mice was about 110 weeks, which was significantly longer than the lifespan of WT mice ($P = 0.0025$ and $P = 0.0067$, respectively) (Fig 2B). Both male and female $Lmna^{LCS/LCS}$ mice demonstrated significantly increased longevity compared to WT mice of the same gender (Supplementary Fig S1A).

Autopsies from $Lmna^{LCS/LCS}$ old mice showed a dramatically increased tumor incidence compared to $Lmna^{LCS/+}$ and $Lmna^{+/+}$ mice (Supplementary Fig S1B). These tumors were primarily located in the abdominal cavity. Histological analysis suggested that they were of lymphoid origin (unpublished results). No visible tumors were detected in younger $Lmna^{LCS/LCS}$ mice (less than a year old), suggesting that lymphomas developed at a late age in these mice. This finding suggests that the $Lmna^{LCS/LCS}$ mice died from the progression of tumors that blunted their lifespan extension.

Consistent with previous observations [10], all of the mice were macroscopically identical before weaning. However, $Lmna^{G609G/G609G}$ mice failed to thrive, in contrast to the other "mutant" mice (Fig 2C). $Lmna^{G609G/G609G}$ mice died at an average of 18 weeks. At 30 weeks of age, $Lmna^{G609G/+}$ mice weighed less than WT and $Lmna^{LCS/+}$ mice, whereas $Lmna^{LCS/LCS}$ mice exhibited an increased weight. The differences between $Lmna^{G609G/+}$ mice and $Lmna^{LCS/LCS}$ mice were most apparent between the ages of 35 and 45 weeks. Moreover, $Lmna^{G609G/+}$ mice in that age range were not yet cachexic. Thus, we used mice in that age group for physiological and molecular biology studies. However, food intake was not significantly different between control and transgenic mice at any age tested (Fig 2C).

Weights of most of the tissues varied in proportion with the body weight. Exceptions were the brain, spleen, and perigonadal white adipose tissue (WAT). Brain size remained constant regardless of the size and genotype of the animals. $Lmna^{LCS/LCS}$ mice accumulated more adipose tissue, whereas $Lmna^{G609G/+}$ mice were extremely lean (Fig 2D). The adipose tissue phenotypes were interesting, as lamin C and progerin might play opposite roles in the homeostasis of this tissue, while having opposing effect on lifespan. The observation on brain weight is discussed in the legend of Supplementary Fig S1C and was not explored further.

Adipose tissue distribution and adipocyte number in $Lmna^{LCS/LCS}$ and $Lmna^{G609G/+}$ mice

Abdominal computed tomography (CT) was performed on 40- to 45-week-old mice. Examination of the subcutaneous and intra-abdominal adipose tissue volumes indicated that all adipose tissue depots were equally affected by the expression of different *Lmna* splicing isoforms (Fig 3A). We calculated the total fat volume per animal and found that $Lmna^{G609G/+}$ mice had a twofold decrease ($P = 0.0255$) in AT volume. In contrast, $Lmna^{LCS/LCS}$ mice showed a 1.5-fold increase ($P = 0.0288$) in AT volume compared to the controls (Fig 3A).

Adjusting adipose tissue weight for body weight did not "correct" for the observed differences. Thus, we examined the potential reason for these discrepancies. The analysis of adipose tissue slices (Fig 3B) suggested that the differences in WAT mass were primarily due to a decrease in the average cell surface for $Lmna^{G609G/+}$ mice and an increase in the average cell surface of $Lmna^{LCS/LCS}$ mice. These results were confirmed by quantification of the surface size of adipocytes from at least five different animals per genotype (Fig 3C). Similar results were obtained with brown adipose tissue slices, where the average cell surface of brown adipocytes for $Lmna^{G609G/+}$ mice was decreased, while it was slightly increased for $Lmna^{LCS/LCS}$ mice (Fig 3B and C).

Preadipocytes from the perigonadal and subcutaneous WAT depots failed to show macroscopic differences in adipocyte differentiation. In addition, we did not observe differences in triglyceride accumulation (Supplementary Fig S2A), nor in the expression of the mature adipocyte markers aP2, Pparg, and Glut4 by RT–qPCR in differentiated preadipocytes (Supplementary Fig S2B). These results suggest that lamin C and progerin are more important for the fate of

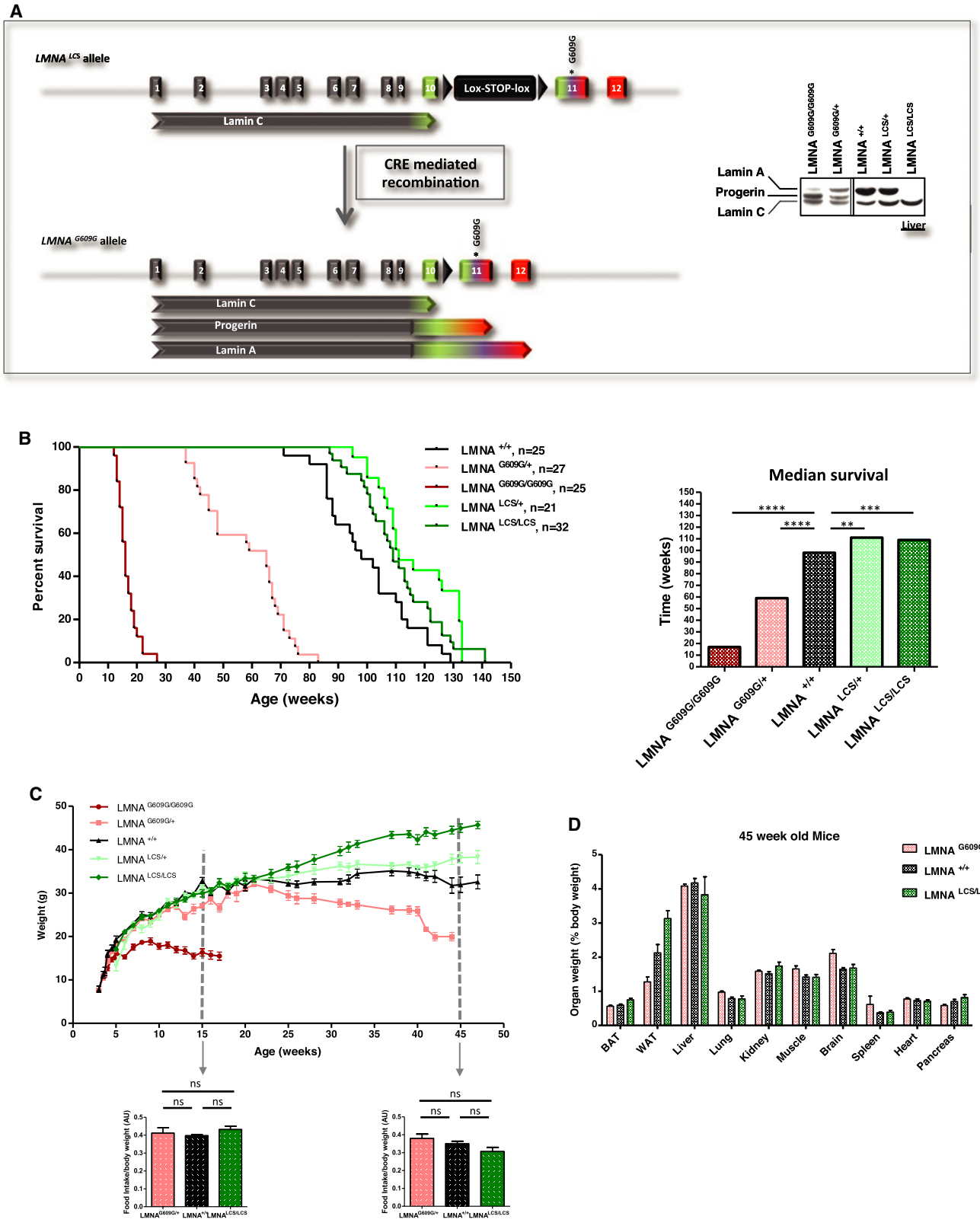

differentiated adipocytes than for preadipocyte differentiation. Furthermore, serum lipoprotein, lipid, and cholesterol profiles did not reveal any significant difference between mice of different genotypes (Supplementary Fig S2C).

Metabolic tests indicated that fasting glycemia was low in *Lmna*$^{G609G/+}$, but not significantly different in *Lmna*$^{LCS/LCS}$ mice compared to WT. Fasting insulin was also significantly decreased in *Lmna*$^{G609G/+}$ mice, while it was increased in normoglycemic

Figure 2. *Lmna* isoforms, progerin and lamin C, affect lifespan and body weight.

A Left panel, structure of the targeted allele after homologous recombination. Right panel, expression levels of lamin A, progerin, and lamin C protein isoforms in the livers of $Lmna^{G609G/G609G}$, $Lmna^{G609G/+}$, $Lmna^{+/+}$, $Lmna^{LCS/+}$, and $Lmna^{LCS/LCS}$, determined by Western blotting.

B Left panel, survival curves of male and female $Lmna^{+/+}$ (n = 25), $Lmna^{G609G/+}$ (n = 27), $Lmna^{G609G/G609G}$ (n = 25), $Lmna^{LCS/+}$ (n = 21), and $Lmna^{LCS/LCS}$ (n = 32) mice. Right panel, histogram showing the median lifespan of each genotype.

C Body weights of male $Lmna^{+/+}$ (n = 11), $Lmna^{G609G/+}$ (n = 9), $Lmna^{G609G/G609G}$ (n = 8), $Lmna^{LCS/+}$ (n = 9), and $Lmna^{LCS/LCS}$ (n = 12) mice. Food intake was measured for 15- and 45-week-old mice (panels below body weight curves).

D Weights of individual organs as a percentage of total body weight for 45-week-old $Lmna^{G609G/+}$ (n = 15), $Lmna^{LCS/LCS}$ (n = 8), and $Lmna^{+/+}$ (n = 10) mice.

Data information: Results were expressed as median (B) or means (C and D) ± s.e.m. The significance of differences in lifespan was determined with the log-rank (Mantel–Cox) test.

$Lmna^{LCS/LCS}$ mice (Fig 3D). $Lmna^{G609G/+}$ mice are more tolerant to glucose, as measured by an intraperitoneal glucose tolerance test (Fig 3E). Glucose tolerance of $Lmna^{LCS/LCS}$ mice is slightly decreased at this age. Moreover, $Lmna^{G609G/+}$ mice are more sensitive to insulin as measured by fasting insulin and by an insulin tolerance test (Fig 3D and F). On the other hand, $Lmna^{LCS/LCS}$ demonstrated mild insulin resistance. High levels of insulin may balance this resistance (Fig 3D). Overall, these results indicate that the $Lmna^{LCS/LCS}$ mice are moderately insulin-resistant, whereas $Lmna^{G609G/+}$ mice are more insulin-sensitive. Increased fat storage and insulin resistance are contrasting with the increased longevity of $Lmna^{LCS/LCS}$ mice, as they are expected to lead progressively to hyperglycemia. Surprisingly, 20-month-old $Lmna^{LCS/LCS}$ mice were rather hypoglycemic (Supplementary Fig S2D), showing that they are able to compensate for obesity and aging-induced insulin resistance, thus highlighting a possible function of lamin C in the maintenance of energy balance.

Energy expenditure and mitochondrial content in $Lmna^{LCS/LCS}$ and $Lmna^{G609G/+}$ mice

Oxygen consumption (VO_2), CO_2 production (VCO_2), respiratory exchange ratios (RER), and energy expenditure were monitored with the Oxymax System. The absolute VO_2 and VCO_2 values are comparable between different genotypes, but when normalized to body weight $Lmna^{G609G/+}$ mice showed a marked increase in VO_2 and VCO_2, whereas $Lmna^{LCS/LCS}$ mice consumed less O_2 and produced less CO_2 (Fig 4A). $Lmna^{G609G/+}$ mice exhibited higher energy expenditure, whereas $Lmna^{LCS/LCS}$ mice exhibited lower energy expenditure. These results indicate that progerin increases the metabolic rate, whereas lamin C reduces overall energy consumption. Interestingly, similar to obese mice, $Lmna^{LCS/LCS}$ mice demonstrated lower RERs, suggesting that they mainly consume fatty acids [13]. The contribution of fat oxidation to energy expenditure calculated from Lusk equations indicated that $Lmna^{LCS/LCS}$ mice burned 80% fat, WT mice used 55% fat, whereas $Lmna^{G609G/+}$ mice consumed only 41% fat. The fact that lamin C-only mice use more fat and less carbohydrates, whereas progerin-expressing mice do the opposite, clearly indicates a prominent role for *Lmna* gene in metabolic fuel partitioning. Interestingly, the amount of mitochondrial DNA was significantly higher in $Lmna^{G609G/+}$ mice and lower in $Lmna^{LCS/LCS}$ mice compared to WT mice (Fig 4B), suggesting global mitochondrial activity. These results were confirmed by the examination of white and brown adipose tissue electron microscopic micrographs (Supplementary Fig S3).

Mouse embryonic fibroblasts (MEFs) derived from $Lmna^{G609G/+}$ and $Lmna^{LCS/LCS}$ embryos exhibited similar variations in mitochondrial DNA content as in the adipose tissues (Fig 4C). Mitochondrial function was studied with a mitochondrial stress test on an XF24 seahorse analyzer. When compared to control MEFs, $Lmna^{G609G/+}$ MEFs showed a basal oxygen consumption rate (OCR) that was 1.5-fold higher, whereas $Lmna^{LCS/LCS}$ MEFs showed a modest but significant decrease in basal respiration (Fig 4D and E). Inhibition of ATP synthesis by oligomycin revealed a significantly higher ATP production in $Lmna^{G609G/+}$ and a decreased ATP production in $Lmna^{LCS/LCS}$ MEFs, but this difference was not significant. FCCP was used to determine the maximal OXPHOS capacity. $Lmna^{G609G/+}$ MEFs showed a 1.13-fold increase in maximal respiration and a 1.3-fold increase in mitochondrial spare capacity, whereas $Lmna^{LCS/LCS}$ showed a 1.4-fold decrease in maximal OCR and a twofold decrease in mitochondrial spare capacity. Proton leak was significantly increased in $Lmna^{G609G/+}$ MEFs and slightly decreased in $Lmna^{LCS/LCS}$ MEFs. The differences in mitochondrial basal and maximal respiration and in proton leak could mainly be due to the differences in mitochondrial number. However, the fact that $Lmna^{G609G/+}$ MEFs have increased spare capacity strongly suggests that their mitochondria were more oxidative. In contrast, the mitochondrial content of $Lmna^{LCS/LCS}$ MEFs was reduced and their mitochondria have less oxidative potential. The results obtained with MEFs are consistent with the global energy expenditure phenotypes of both $Lmna^{G609G/+}$ and $Lmna^{LCS/LCS}$ mice. The reduction in oxidative capacity of the adipose tissue is expected to lead to the obese phenotype of $Lmna^{LCS/LCS}$ mice that have less capacity to burn lipids and therefore gain more weight.

Gene expression analysis of adipose tissue samples from $Lmna^{LCS/LCS}$ and $Lmna^{G609G/+}$ mice

PGC1a (Ppargc1a) is a master regulator of mitochondrial biogenesis [14–16]. UCP1 (uncoupling protein 1) is a PGC1a target gene and a key thermogenic protein. Induced expression of UCP1 in WAT reduces obesity and improves insulin sensitivity [14,17]. The expression in adipose tissue of PGC1a and UCP1, both at RNA (Fig 5A) and protein (Fig 5B) levels, varied in opposite ways in mice expressing progerin versus mice expressing lamin C alone. Changes in mitochondrial gene expression might thus be responsible for the observed differences in energy consumption and expenditure. RT–qPCR analysis of PGC1a target genes (*Tfam*, *NRF1*, *SOD2*, and *NRF2*), electron transport chain (ETC) genes (*ATP synthase*, *SDHA*, *cytochrome C oxidase*, and *NADPH dehydrogenase*), and fatty oxidation genes (*mCAD* and *CPT2*) showed that expression of each gene

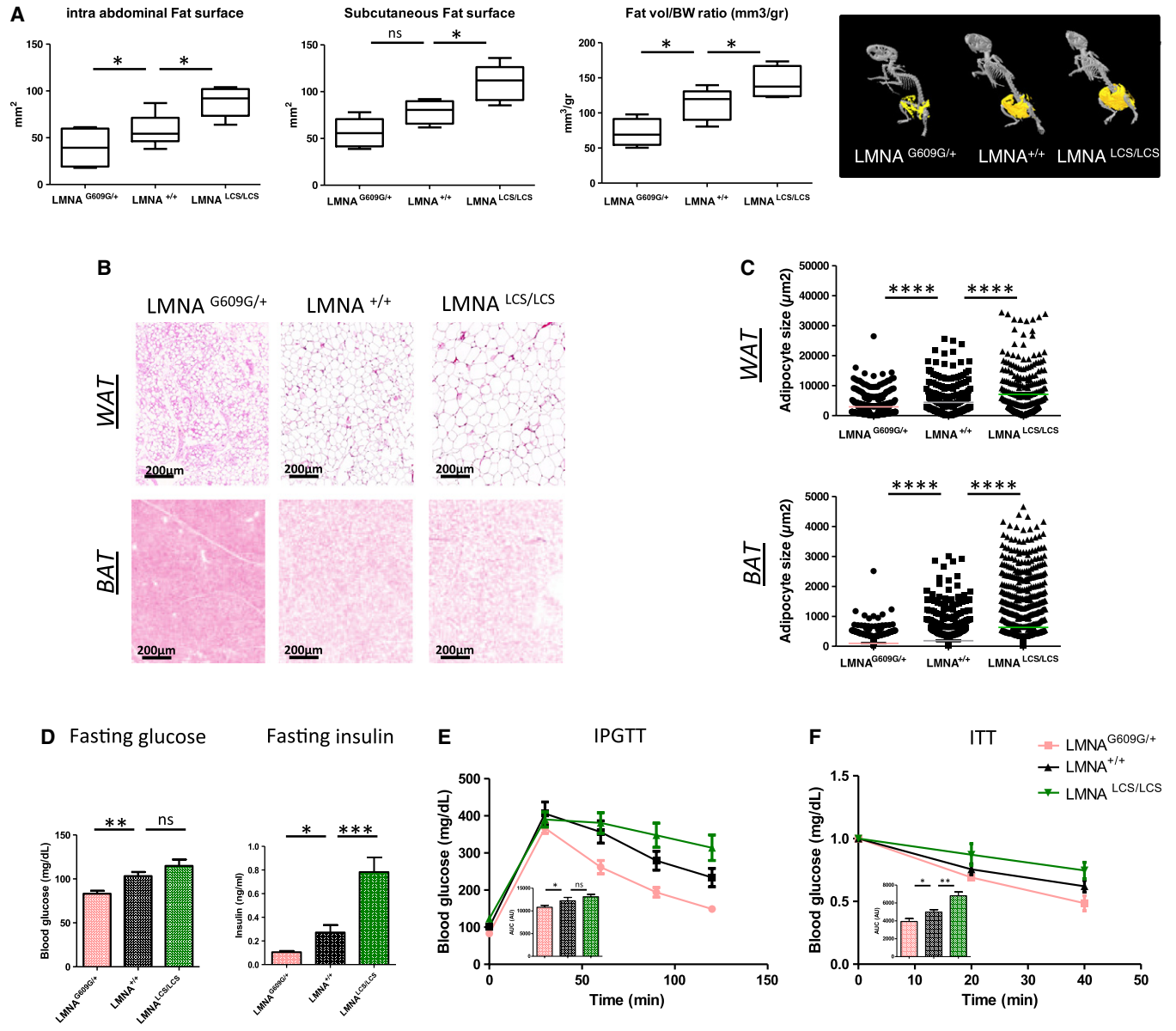

Figure 3. Antagonistic adipose tissue alterations in *Lmna*$^{G609G/+}$ and *Lmna*$^{LCS/LCS}$ mice.

A PET-CT imaging analysis showing quantification of subcutaneous fat surface, intra-abdominal fat surface, and total fat volume normalized to body weight in *Lmna*$^{G609G/+}$, *Lmna*$^{+/+}$, *Lmna* $^{LCS/LCS}$ mice (n = 5 per genotype). A representative PET-CT image for each genotype is shown in the right panel.

B Representative images of HE-stained sections of WAT (upper panels) and BAT (lower panels) from *Lmna*$^{+/+}$, *Lmna*$^{G609G/+}$, and *Lmna*$^{LCS/LCS}$ mice.

C Quantification of adipocyte size from WAT (upper panel) and BAT (lower panel) with ImageJ software (n = 5 per genotype).

D Metabolic measurements (fasting glucose and insulin, intraperitoneal glucose tolerance test and insulin tolerance test) of *Lmna*$^{+/+}$ (n = 6), *Lmna*$^{G609G/+}$ (n = 10), and *Lmna*$^{LCS/LCS}$ (n = 7) mice. Area under the curve for IPGTT and ITT was analyzed (AUC).

Data information: All experiments were conducted using 45-week-old male mice. Results were expressed as means ± s.e.m. The significance of differences was determined with the Student's t-test.

[17], except for *NRF2*, varied inversely between *Lmna*$^{LCS/LCS}$ and *Lmna*$^{G609G/+}$ samples (Fig 5C), suggesting that LMNA isoforms affect mitochondrial gene expression.

In order to determine the molecular pathways altered by lamin C and progerin expression and their roles in energy metabolism and aging, we analyzed the WAT transcriptome in control mice and in *Lmna*$^{G609G/G609G}$ and *Lmna*$^{LCS/LCS}$ mice, as examples of the most extreme aging phenotypes. We used samples from fasting 4-month-old male mice to probe Affymetrix exon arrays (results are accessible at https://www.easana.com/). Consistent with the essential role of lamins in nuclear architecture, WAT samples from *Lmna*$^{G609G/G609G}$ mice demonstrated extreme variations, with 6,509 up-regulated and 3,024 down-regulated mRNAs. Large variations were also observed at the level of alternative splicing, confirming recent observations

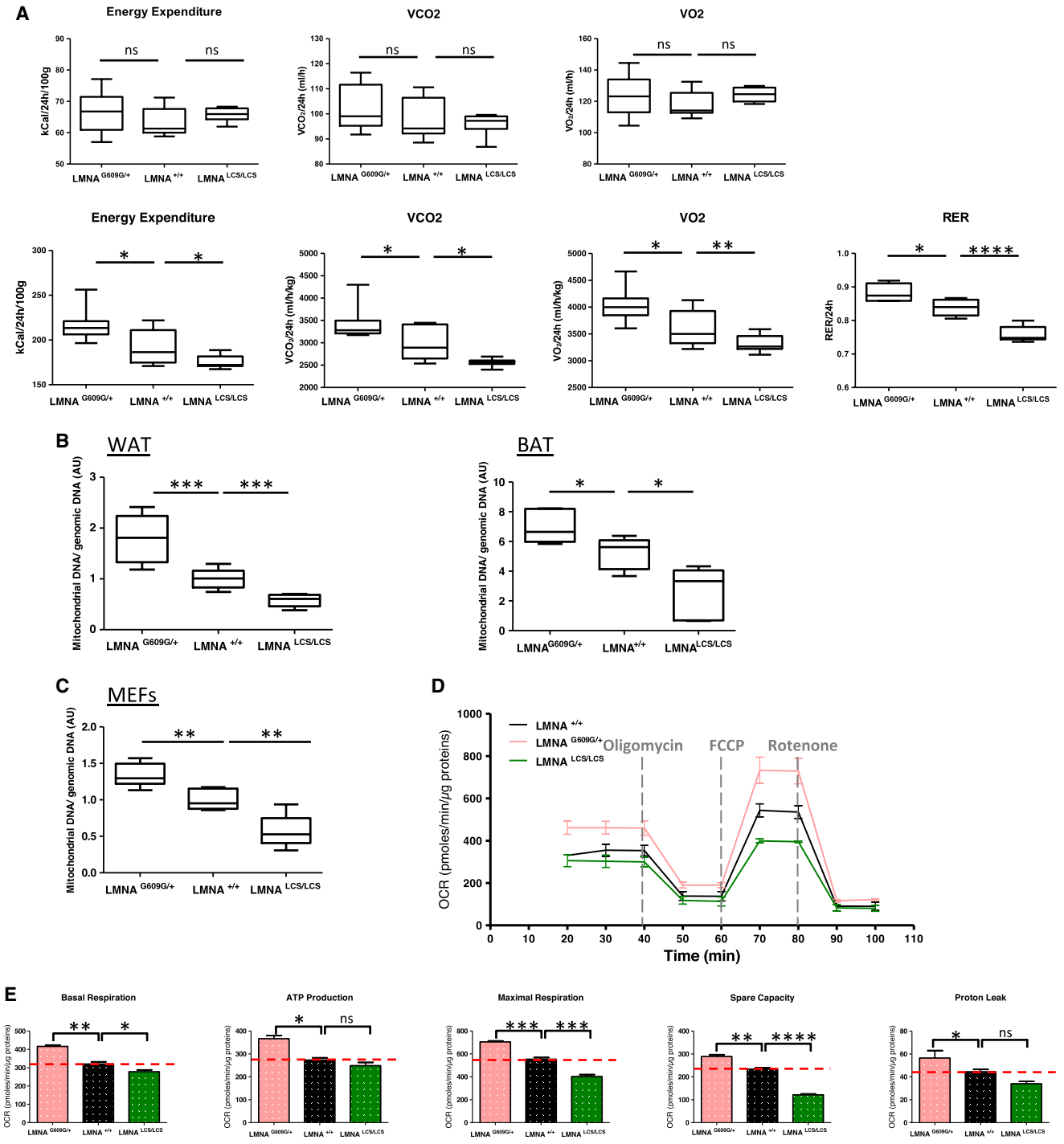

Figure 4. ***LMNA*** **isoforms modify energy expenditure and mitochondrial content in mice and in MEFs.**

A Upper panels correspond to absolute values of VCO_2, VO_2, RER, and energy expenditure. Lower panels represent the same values normalized to body weight (n = 5 per genotype).

B Mitochondrial DNA levels in WAT and BAT were assessed by qPCR and normalized to genomic DNA (n = 7 per genotype).

C Mitochondrial DNA levels in MEFs were assessed by qPCR and normalized to genomic DNA (n = 4 clones per genotype).

D, E MEFs oxygen consumption rates (OCR) were determined with a Seahorse XF24 Flux analyzer in basal and stimulated conditions (n = 3 clones per genotype). The areas under the curve from different sections of the experiment are shown as individual histograms (E) for basal respiration, ATP production, maximal respiration, mitochondrial spare capacity, and proton leak.

Data information: Results were expressed as means ± s.e.m. The significance of differences was determined with the Student's t-test. See Supplementary Table S1 for a list of primers used for RT–qPCR.

that progerin expression triggers a senescent phenotype characterized by large changes in alternative splicing [18,19]. WAT samples from $Lmna^{LCS/LCS}$ mice showed also large variations, with 736 up-regulated and 1,563 down-regulated genes, and different alternative splicing of 2,691 exons (https://www.easana.com/). These observations are consistent with a recent finding showing that lamin A/C interacts with distinct spatially restricted subpromoter regions associated with distinct transcriptional outcomes in human adipose tissue stem cells [18,20].

Variations in gene expression may directly or indirectly contribute to the different phenotypes elicited by lamin C and progerin. We focused on 278 annotated genes (https://www.easana.com/), for which inverse expression patterns existed between the two phenotypes. Interestingly, KEGG pathway analysis of those genes showed that two of the three most regulated pathways are involved in energy metabolism (arachidonic acid metabolism and glycerolipid metabolism, Fig 5D). These data also confirmed that PGC1a was one of the inversely regulated genes, further validating our approach (Fig 5E). In addition to PGC1a, 29 genes involved in lipid metabolism were identified with expression controlled in an inverse way by lamin C and progerin. These 30 genes could be involved in the process of aging (Fig 5E).

We used dedicated qPCR arrays (Adipogenesis and Fatty acid metabolism RT² Profiler™ PCR Arrays) designed to study 84 genes per pathway to further confirm these results (Supplementary Fig S4A and B). Only six genes showed inverse expression on both arrays (*Ppargc1a*, *Lep*, *Sfrp5*, *Acot3*, *Acsm3*, and *Bdh2*). Four (*Ppargc1a*, *Lep*, *Sfrp5*, and *Acsm3*) were already on the list of 30 genes obtained from the Affymetrix analysis. Thus, these four genes were considered candidate genes accounting for the phenotypes associated with the lamin isoforms. Interestingly, 29 of 84 genes involved in the regulation of fatty acid metabolism were up-regulated in the adipose tissue from progeria mice. In contrast, all of the genes that we examined in this pathway (8 out of 84) were down-regulated in the adipose tissue from lamin C-only mice, further confirming that these two lamin isoforms have antagonistic functions in the regulation of fatty acid metabolism (Supplementary Fig S4B).

One of the four candidate genes, *Sfrp5* suppresses oxidative metabolism, is strongly induced during adipocyte differentiation, and is up-regulated in adipocytes during obesity and likely counteracts WNT signaling [21]. Moreover, *SFRP5*-deficient mice are phenotypically similar to $Lmna^{G609G/+}$ mice (same numbers of adipocytes but fewer large adipocytes and increased mitochondrial activity, partially mediated by PGC1a). However, changes in leptin expression cannot explain the metabolic phenotypes, since increased expression of leptin in $Lmna^{LCS/LCS}$ mice would result in reduced food intake and increased energy expenditure. While increased adipose tissue mass is always correlated with leptin expression, $Lmna^{LCS/LCS}$ mice display only slight decrease in food intake that is not statistically significant, suggesting that the increase in the expression of *leptin* mRNA is not sufficient to increase circulating leptin levels. Alternatively, $Lmna^{LCS/LCS}$ mice are leptin resistant.

Concluding remarks

Our results support the notion that RNA processing of the *Lmna* gene is an active conserved mechanism that contributes to metabolic adaptations of adipose tissue in mammals. While some of the phenotypes of $Lmna^{LCS/LCS}$ mice are contrasting with their increased longevity, both in MEFs and mice, lamin C-only expression results in low mitochondrial activity, whereas progerin expression strongly increases organelle activity. Strikingly, these distinct effects on mitochondrial activity correlate with opposing effects of these lamins on lifespan. Although these could be independent phenotypes, recent studies have linked mitochondrial function to lifespan [22]. The finding that old $Lmna^{LCS/LCS}$ mice are able to compensate for deleterious effects triggered by obesity suggests that lamin C protects against increased oxidative stress associated with fat accumulation [23]. In contrast, progerin increases energy expenditure and mitochondrial activity, which probably induces potent oxidative stress, characteristic of senescence [24–26] and one of the central hallmarks of the normal aging process [26]. The lamin isoforms by changing the nuclear envelope architecture may also contribute to changes in the expression of genes involved in mitonuclear imbalance controlling longevity.

Materials and Methods

Database searches and sequence analysis

Lamin A/C gene sequences were retrieved from Ensembl (http://www.ensembl.org/) and aligned with MAFFT in the Geneious package (v 6.1.5 created by Biomatters, available from http://www.geneious.com/).

The occurrence of lamin A/C ESTs in databases was determined with BLAST (http://blast.ncbi.nlm.nih.gov) using protein and nucleic acid queries specific for either of the lamin isoforms (exon 11 for lamin A, intron 10 for lamin C) or for a sequence common to both isoforms (other exons). A more detailed description of sequence analysis can be found in Supplementary Methods.

Figure 5. Gene expression profiling of WAT adipose tissue from *Lmna* mutant mice.

A Relative mRNA levels of *PGC1*a and *UCP1* in WAT were determined by RT–qPCR.

B Protein levels of PGC1a and UCP1 in WAT were determined by Western blotting. Lamin A/C levels and γ-tubulin levels were used as controls.

C Relative mRNA levels of mitochondrial markers in WAT were assessed by RT–qPCR.

D Table representing KEGG pathways significantly and antagonistically regulated by progerin and lamin C derived from exon array analysis of WAT from 18-week-old $Lmna^{G609G/G609G}$ and $Lmna^{LCS/LCS}$ mice (n = 5 per genotype).

E Metabolic genes that are oppositely regulated in WAT from 18-week-old $Lmna^{G609G/G609G}$ and $Lmna^{LCS/LCS}$ mice versus $Lmna^{+/+}$ mice (n = 5 per genotype). Up-regulated genes are in red boxes, and down-regulated genes are in green boxes.

Data information: RT–qPCR and WB were performed with 45-week-old $Lmna^{+/+}$, $Lmna^{G609G/+}$, and $Lmna^{LCS/LCS}$ mice samples (n = 5 per genotype). Results were expressed as means ± s.e.m. The significance of differences was determined with the Student's t-test. See Supplementary Table S1 for a list of primers used for RT–qPCR.

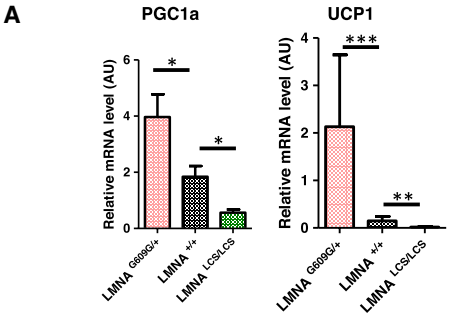

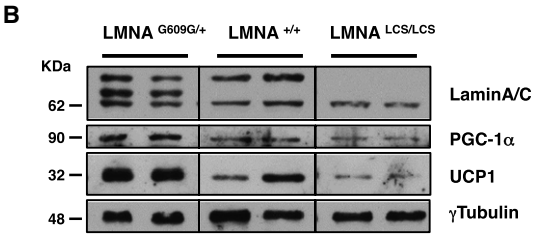

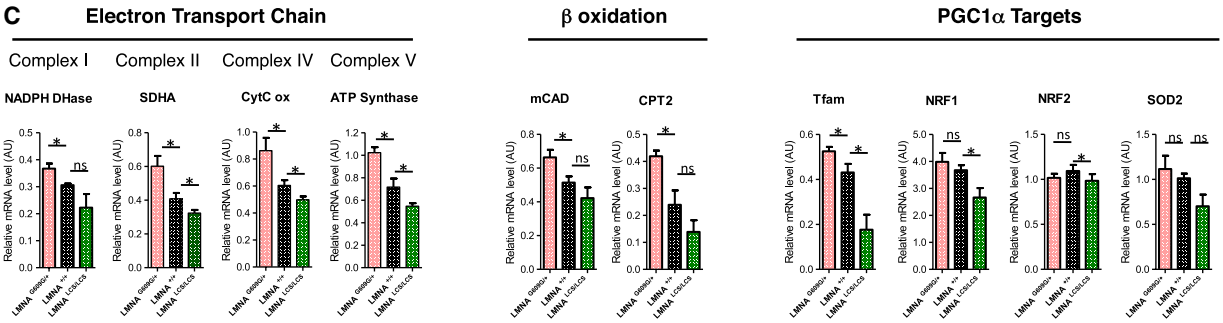

D

Significant Pathways (10)

KEGG Pathway ID	Pathway Description (KEGG)	Nb Genes in Pathway	Nb Genes regulated in Pathway	P-Value	% of regulated genes
mmu04610	Complement and coagulation cascades	75	7	$6{,}08.10^{-4}$	9,33
mmu00590	Arachidonic acid metabolism	83	6	$6{,}08.10^{-3}$	7,23
mmu04270	Vascular smooth muscle contraction	120	7	$6{,}66.10^{-3}$	5,83
mmu05414	Dilated cardiomyopathy	92	6	$9{,}34.10^{-3}$	6,52
mmu00561	Glycerolipid metabolism	47	4	$2{,}81.10^{-2}$	8,51
mmu04512	ECM-receptor interaction	83	5	$2{,}92.10^{-2}$	6,02
mmu05410	Hypertrophic cardiomyopathy (HCM)	84	5	$3{,}03.10^{-2}$	5,95
mmu05416	Viral myocarditis	94	5	$4{,}31.10^{-2}$	5,32
mmu00564	Glycerophospholipid metabolism	67	4	$6.82.10^{-2}$	5,97
mmu05412	Arrhythmogenic right ventricular cardiomyopathy (ARVC)	75	4	$8{,}88.10^{-2}$	5,33

E

Protein	G609G/G609G vs +/+		LCS/LCS vs +/+		Function
	Fold change	P-value	Fold change	P-value	
Lep	33.09	9.90E-08	2.11	3.87E-05	Leptin plays a key role in regulating energy intake and energy expenditure, including appetite/hunger and metabolism
Cyp4f18	1.68	1.58E-03	2.22	9.36E-04	Belongs to Cyp4 family of enzymes that catalyze the oxidation of fatty acid
Sod3	3.61	1.19E-04	1.84	8.54E-03	This gene encodes a member of the superoxide dismutase (SOD) protein family that play a key antioxidant role
Gcnt4	5.58	1.58E-05	1.74	6.63E-04	Belongs to the family of acyltransferases that participates to aminosugar metabolism
Mrps6	2	1.39E-02	1.75	6.20E-03	Mammalian mitochondrial ribosomal proteins are encoded by nuclear genes and help in protein synthesis within the mitochondrion
Sfrp5	14.79	3.25E-04	2.83	6.97E-04	Sfrp5 is an anti-inflammatory adipokine that modulates metabolic dysfunction in obesity
Dgat2	6.5	1.90E-05	1.63	2.38E-04	This gene encodes one of two enzymes that catalyzes the final reaction of triglycerides synthesis
Slc1a1	5.52	1.09E-06	1.8	1.00E-04	Plays an essential role in transporting glutamate (a key compound in cellular metabolism) across plasma membranes
Lpgat1	5.28	1.74E-05	1.65	7.42E-03	catalyzes the reacylation of LPG to phosphatidylglycerol, a phospholipid that is an important precursor for the synthesis of cardiolipin
Pnpla3	3.38	1.96E-05	1.95	2.25E-05	Also known as Adiponutrin, a lipase that mediates triacylglycerol hydrolysis in adipocytes and may be involved in the balance of energy usage/storage in adipocytes
Paqr9	3.24	1.58E-03	1.6	2.73E-02	Receptor of adiponectin, which is an adipokine that modulates glucose metabolism and fatty acid oxidation
Hgfac	3.05	4.59E-04	1.87	9.99E-05	Acts as a serine protease that converts hepatocyte growth factor from his precursor to his active form
Pla2g5	2.93	1.40E-03	2.61	6.16E-05	Catalyzes the hydrolysis of membrane phospholipids to generate lysophospholipids and free fatty acids including arachidonic acid.
Dhcr24	2.87	1.64E-05	1.71	1.18E-04	Encodes a (FAD)-dependent oxidoreductase which catalyzes the reduction of the delta-24 double bond of sterol intermediates during cholesterol biosynthesis
Lipf	2.84	8.43E-04	2	2.20E-03	Gastric lipase involved in the digestion of triglycerides in the gastrointestinal tract, responsible for 30% of fat digestion processes occurring in human
Sfrp4	2.67	8.84E-04	1.73	6.11E-05	Secreted Frizzled-Related Protein 4 reduces insulin secretion and is overexpressed in Type 2 Diabetes
Slc7a5	2.58	4.09E-07	1.62	1.01E-04	Involved in cellular amino-acid uptake
Igfals	2.43	3.57E-02	1.68	4.46E-03	Crucial role in determining the endicrine effect of IGF on target tissues
Dhrs3	2.2	1.39E-04	1.65	1.04E-04	p53-Inducible DHRS3 is an endoplasmic reticulum protein associated with lipid droplet accumulation
Alox15	1.67	2.04E-04	1.95	1.62E-03	Lipoxygenases (LOXs) are a family of non-heme iron dioxygenases that participates in arachidonic acid metabolism and linoleic acid metabolism.
Gpd1	1.95	4.36E-05	1.66	3.78E-05	The encoded protein plays a critical role in carbohydrate and lipid metabolism
Akr1b7	2.08	6.27E-05	10.79	2.20E-03	Induced in response to oxidative stress
Pgam2	3.98	1.95E-04	3.94	6.40E-04	Phosphoglycerate mutase (PGAM) catalyzes the reversible reaction of 3-phosphoglycerate (3-PGA) to 2-phosphoglycerate
Scd3	5.25	1.79E-05	2.72	8.63E-04	Stearoyl-coenzyme A (CoA) desaturase (SCD) is a key enzyme involved in the conversion of saturated fatty acids into monounsaturated fatty acids
Ptgs2	3.86	6.30E-07	2.77	1.20E-04	Prostaglandin endoperoxide H synthase, COX 2, converts arachidonic acid (AA) to prostaglandin endoperoxide H2
Cyp4a12b	1.67	1.01E-02	4.93	4.99E-04	Belongs to Cyp4 family of enzymes that catalyze the oxidation of fatty acid
Acsm3	1.94	7.63E-05	1.61	4.84E-04	Has medium-chain fatty acid:CoA ligase activity. The protein is activated by the deacetylation of lysine residues of the active site by Sirt3.
Slc38a4	1.74	1.86E-03	2.4	1.04E-04	Sodium-dependent amino acid transporter. Mediates electrogenic symport of neutral amino acids and sodium ions
Fabp3	1.52	1.21E-02	2.31	1.04E-02	H-FABP (FABP3) is involved in active fatty acid metabolism where it transports fatty acids from the cell membrane to mitochondria for oxidation
Ppargc1a	2.07	6.30E-05	1.58	8.78E-03	Transcription coactivator that plays a central role in the regulation of cellular energy metabolism

Animal experiments & ethics statement

Transgenic mice ($LMNA^{G609G/+}$ and $LMNA^{LCS/LCS}$) were generated as previously described [10]. A more detailed description of the breeding strategy, tumor evaluation, micro-computed tomography, metabolic evaluation, and Oxymax analysis can be found in Supplementary Methods.

All animal procedures were conducted in strict adherence with the European Community Council Directive of November 24, 1986 (86-609/EEC). Mice were maintained in pathogen-free conditions in our animal facility (E34-172-16). All experiments were conducted by authorized personnel (agreements JT 34-236; MDT 34-433; IL-M 34-467; KC 34-028; CC has legal training) and approved by the Institutional Review Board at the Animal Facility of the Institut de Génétique Moléculaire de Montpellier (agreement no CEEA-LR-12112).

Food intake was measured three times over a period of 72 h with seven animals per genotype in individual cages.

Microarray data analysis

All the data are deposited in GEO (NCBI) under accession number GSE51204. Affymetrix Mouse Exon 1.0 ST arrays were hybridized by GenoSplice technology (www.genosplice.com) according to their standard protocol. A detailed description of the procedure can be found in Supplementary Methods.

Statistical analysis

The survival curves were completed using the Kaplan–Meier curve. The median survival is representative of the survival curves. We use the log-rank (Mantel–Cox) test to perform the statistical analyses of the survival curves.

All the other results were expressed as means ± standard error of the means (s.e.m.). The significance of differences was determined with the Student's *t*-test, with significance defined as $P < 0.05$ ($^{*}P < 0.05$, $^{**}P < 0.005$, $^{***}P < 0.0005$, $^{****}P < 0.00005$).

Supplementary information for this article is available online: http://embor.embopress.org

Acknowledgements

This work was supported by grants from Fondation pour la Recherche Médicale and Splicos Therapeutics. JT is senior member of the Institut Universitaire de France. We are grateful to N. Levy and C. Lopez-Otin for providing $Lmna^{LCS/+}$ mice and the Montpellier-RIO imaging platform (Montpellier, France), to the Histology Experimental Network of Montpellier, to the "Centre de Ressources en Imagerie Cellulaire de Montpellier" (France), and to the IGMM animal facilities. The authors are grateful to C. Cazevieille and C. Sanchez for their technical assistance and P. de la Grange from Genosplice. I.L-M. was supported by a graduate fellowship from the Ministère Délégué à la Recherche et aux Technologies and CNRS. C. L-H is supported by ITN RNPnet Grant.

Author contributions

ICLM and MDT performed most of the experiments and contributed to writing the manuscript. CC performed the metabolic data and contributed to writing the paper. LL performed the qPCR experiments. EZA, GB, and FC contributed to CT scan and metabolic cages experiments. PC contributed to histological data. PF and KC have made the sequence alignment. LF provided critical metabolic discussions. JT designed the study and wrote the manuscript.

Conflict of interests

The authors declare that they have no conflict of interest.

References

1. Bishop NA, Guarente L (2007) Genetic links between diet and lifespan: shared mechanisms from yeast to humans *Nat Rev Genet* 8: 835 – 844
2. Kenyon C (2005) The plasticity of aging: insights from long-lived mutants *Cell* 120: 449 – 460
3. Houtkooper RH, Williams RW, Auwerx J (2010) Metabolic networks of longevity *Cell* 142: 9 – 14
4. Hennekam RCM (2006) Hutchinson-Gilford progeria syndrome: review of the phenotype *Am J Med Genet A* 140: 2603 – 2624
5. De Sandre-Giovannoli A, Bernard R, Cau P, Navarro C, Amiel J, Boccaccio I, Lyonnet S, Stewart CL, Munnich A, Le Merrer M et al (2003) Lamin a truncation in Hutchinson-Gilford progeria *Science* 300: 2055
6. Eriksson M, Brown WT, Gordon LB, Glynn MW, Singer J, Scott L, Erdos MR, Robbins CM, Moses TY, Berglund P et al (2003) Recurrent *de novo* point mutations in lamin A cause Hutchinson-Gilford progeria syndrome *Nature* 423: 293 – 298
7. Lopez-Mejia IC, Vautrot V, De Toledo M, Behm-Ansmant I, Bourgeois CF, Navarro CL, Osorio FG, Freije JMP, Stévenin J, De Sandre-Giovannoli A et al (2011) A conserved splicing mechanism of the LMNA gene controls premature aging *Hum Mol Genet* 20: 4540 – 4555
8. Bergo MO, Gavino B, Ross J, Schmidt WK, Hong C, Kendall LV, Mohr A, Meta M, Genant H, Jiang Y et al (2002) Zmpste24 deficiency in mice causes spontaneous bone fractures, muscle weakness, and a prelamin A processing defect *Proc Natl Acad Sci USA* 99: 13049 – 13054
9. Fong LG, Ng JK, Lammerding J, Vickers TA, Meta M, Coté N, Gavino B, Qiao X, Chang SY, Young SR et al (2006) Prelamin A and lamin A appear to be dispensable in the nuclear lamina *J Clin Invest* 116: 743 – 752
10. Osorio FG, Navarro CL, Cadiñanos J, Lopez-Mejia IC, Quirós PM, Bartoli C, Rivera J, Tazi J, Guzmán G, Varela I et al (2011) Splicing-directed therapy in a new mouse model of human accelerated aging *Sci Transl Med* 3: 106ra107
11. Peter A, Reimer S (2012) Evolution of the lamin protein family: what introns can tell *Nucleus* 3: 44 – 59
12. Pendás AM, Zhou Z, Cadiñanos J, Freije JMP, Wang J, Hultenby K, Astudillo A, Wernerson A, Rodríguez F, Tryggvason K et al (2002) Defective prelamin A processing and muscular and adipocyte alterations in Zmpste24 metalloproteinase-deficient mice *Nat Genet* 31: 94 – 99
13. Martin TL, Alquier T, Asakura K, Furukawa N, Preitner F, Kahn BB (2006) Diet-induced obesity alters AMP kinase activity in hypothalamus and skeletal muscle *J Biol Chem* 281: 18933 – 18941
14. Fisler JS, Warden CH (2006) Uncoupling proteins, dietary fat and the metabolic syndrome *Nutr Metab (Lond)* 3: 38
15. Handschin C, Spiegelman BM (2006) Peroxisome proliferator-activated receptor gamma coactivator 1 coactivators, energy homeostasis, and metabolism *Endocr Rev* 27: 728 – 735
16. Finck BN, Kelly DP (2006) PGC-1 coactivators: inducible regulators of energy metabolism in health and disease *J Clin Invest* 116: 615 – 622

17. Austin S, St-Pierre J (2012) PGC1α and mitochondrial metabolism–emerging concepts and relevance in ageing and neurodegenerative disorders *J Cell Sci* 125: 4963 – 4971
18. Lund E, Oldenburg A, Delbarre E, Freberg C, Duband-Goulet I, Eskeland R, Buendia B, Collas P (2013) Lamin A/C-promoter interactions specify chromatin state-dependent transcription outcomes *Genome Res* 23: 1580 – 1589
19. Cao K, Blair CD, Faddah DA, Kieckhaefer JE, Olive M, Erdos MR, Nabel EG, Collins FS (2011) Progerin and telomere dysfunction collaborate to trigger cellular senescence in normal human fibroblasts *J Clin Invest* 121: 2833 – 2844
20. Miranda M, Chacón MR, Gutiérrez C, Vilarrasa N, Gómez JM, Caubet E, Megía A, Vendrell J (2008) LMNA mRNA expression is altered in human obesity and type 2 diabetes *Obesity* 16: 1742 – 1748
21. Mori H, Prestwich TC, Reid MA, Longo KA, Gerin I, Cawthorn WP, Susulic VS, Krishnan V, Greenfield A, Macdougald OA (2012) Secreted frizzled-related protein 5 suppresses adipocyte mitochondrial metabolism through WNT inhibition *J Clin Invest* 122: 2405 – 2416
22. Houtkooper RH, Mouchiroud L, Ryu D, Moullan N, Katsyuba E, Knott G, Williams RW, Auwerx J (2013) Mitonuclear protein imbalance as a conserved longevity mechanism *Nature* 497: 451 – 457
23. Bondia-Pons I, Ryan L, Martinez JA (2012) Oxidative stress and inflammation interactions in human obesity *J Physiol Biochem* 68: 701 – 711
24. Fischer F, Hamann A, Osiewacz HD (2012) Mitochondrial quality control: an integrated network of pathways *Trends Biochem Sci* 37: 284 – 292
25. Bratic A, Larsson N-G (2013) The role of mitochondria in aging *J Clin Invest* 123: 951 – 957
26. Lopez-Otin C, Blasco MA, Partridge L, Serrano M, Kroemer G (2013) The hallmarks of aging *Cell* 153: 1194 – 1217